Suplemento de la Revista Mexicana de Física **4** 021102 (2023) 1–5

QCD phase diagram in the presence of electric and magnetic fields

Aftab Ahmad

Institute of Physics, Gomal University, 29220, D.I. Khan, Khyber Pakhtunkhaw, Pakistan.

Received 15 January 2022; accepted 4 May 2022

In this contribution, We revisit the effect of electric eE and magnetic field eB and on the critical temperature $T_c^{\chi,C}$ of the chiral symmetry breaking/restoration and confinement/deconfinement phase transition in the QCD Phase diagram. In this context, we use the symmetry-preserving vector-vector contact interaction model of quarks, in the Schwinger-Dyson equations framework and in the proper time regularization scheme. We also describe the phenomenon of inverse electric catalysis in the pure electric case, magnetic catalysis (and inverse magnetic catalysis) in the pure magnetic case and inverse electromagnetic catalysis in the presence of both electric and magnetic background fields.

Keywords: Schwinger Dysons Eqautions; chiral symmetry breaking; confinement; electric and magnetic fields; QCD phase diagram.

DOI: https://doi.org/10.31349/SuplRevMexFis.4.021102

1. Introduction

Quantum chromodynamics (QCD) is a well-known theory of the strong color interaction among quarks and gluons with its two important properties: the asymptotic freedom (high energy domain) which can be tackled with Feynman-based perturbation methods and the quark confinement (low energy) which can be handled with the non-perturbative techniques of QCD. The Dynamical chiral symmetry breaking is another important of non-perturbative QCD which is related to the generation of dynamical quark masses. It is well known that the fundamental degrees of freedom (QCD) at zero or low temperature T, is the low energy hadrons. Whereas at sufficiently high T, the interactions become weak, causing hadrons to melt down to a phase where quarks and gluons become the new degrees of freedom. The deconfinement of quarks occurs and the dynamical chiral symmetry restores in this new phase. The situation becomes more interesting when the hadronic matter is subjected to an external electric and magnetic field. It yields a significant impact on phase transition. In the pure magnetic case at zero temperature, the strong magnetic field tends to enhance the formation of quark anti-quark condensate and the dynamical mass increase as we increase eB, this phenomenon in the literature dubbed as *magnetic catalysis* (MC) [1–8]. Even at finite temperature T the magnetic catalysis predicted, i. e., the pseudo-critical temperature $T_c^{\chi,C}$ (where the superscript χ indicates chiral symmetry breaking-restoration, C refers to confinement-deconfinement, and the subscript c stands for criticality) is increased with an increase in eB [1, 2, 4, 9]. However, in the past few years, the lattice QCD Simulation [10–12] predicted that at finite T, the $T_c^{\chi,C}$ is decreases with the increase of eB, such a phenomenon is referred to as *the inverse magnetic catalysis* (IMC). such a phenomenon is also supported by low-energy QCD models by using the magnetic field dependent coupling (*i.e.,* monotonically decreasing function with the magnetic field) [13–19]. In contrast to the magnetic field background, the strong electric field suppresses the dynamically generated quark masses and formation of a quark-antiquark condensate and thus restores the chiral symmetry, such a phenomenon is usually referred to as the chiral electric inhibition effect [1, 2, 9, 18, 20–23], or the chiral electric rotation effect [24]. At finite T, the pseudo-critical temperature $T_c^{\chi,C}$ for the chiral phase transition decreases with an increase of electric field eE and is dubbed as the *inverse electric catalysis* (IEC) [22, 25]. In heavy-ion collisions experiments, the electric and magnetic fields produced with the same order of magnitude ($\sim 10^{18}$ to 10^{20}G) [26–29] in the event-by-event collisions using Au + Au at RHIC-BNL, and in a non-central heavy-ion collision of Pb + Pb in ALICE-LHC. Upon considering the effect of both electric field and magnetic field on the chiral phase transition paid much attention to the exploration of the above-mentioned phenomenon in the low energy effective models [22, 24, 30, 31].

In this manuscript, we discuss the phenomena of magnetic catalysis/inverse catalysis, inverse electric catalysis and electromagnetic inverse catalysis in the presence of external electric and magnetic fields. The detailed analysis and discussion on the subject are found in Ref. [18]. Here, we just outline the general formalism and expressions in the presence of background fields and describe how the results can be obtained. Our unified framework in this work is based on the Schwinger-Dyson equations (SDE) in the rainbow-ladder truncation, in the Landau gauge, the symmetry preserving confining vector-vector contact interaction model (CI) [32], and the Schwinger proper time regularization scheme [33].

This article is organized as follows. In Sec. 2, we present the general formalism of the contact interaction model. In Sec. 3, We set up the gap equation in the presence of background fields. in Sec. 4. We sketch the phase diagram at finite temperatures and in the presence of background fields. The last Sec. 5 is devoted to the conclusion.

2. General formalism

The Schwinger-Dyson's equations (SDE) for dressed-quark propagator S, are given by:

$$S^{-1}(p) = i\gamma \cdot p + m + \Sigma(p), \tag{1}$$

with

$$\Sigma(p) = \int \frac{d^4k}{(2\pi)^4} g^2 \Delta_{\mu\nu}(p-k) \times \frac{\lambda^a}{2}\gamma_\mu S_{(k)} \frac{\lambda^a}{2}\Gamma_\nu(p,k)\,, \tag{2}$$

is the quark self-energy. g is the coupling constant, and m is the current quark mass. The λ^a's are the usual Gell-Mann matrices, Γ_ν is the dressed quark-gluon vertex, $\Delta_{\mu\nu}$ is the gluon propagator.

The symmetry preserving four-fermions vector-vector contact interaction (CI) model with a finite gluon mass [34] in the Landau gauge and the rainbow ladder truncation is given by:

$$g^2\Delta_{\mu\nu}(k)\Gamma_\nu(p,k) = \delta_{\mu\nu}\frac{4\pi\alpha_{\rm ir}}{m_G^2} \equiv \delta_{\mu\nu}\alpha_{\rm eff}\gamma_\nu\,, \tag{3}$$

where $m_G = 800$ MeV is the gluon mass scale [35, 36] and the parameter $\alpha_{\rm ir} = 0.93\pi$ is the infrared-enhanced interaction strength. Using the CI model Eq. (3) in Eq. (1), and performing the "Trace" over Lorentz and color matrices, we have the gap equation:

$$M = m + \frac{4\alpha_{\rm eff}}{3}\int^{\Lambda} \frac{d^4k}{(2\pi)^4}{\rm Tr}[S_(k)]\,. \tag{4}$$

The Eq. (4) can be further simplified as

$$M = m + \frac{16\alpha_{\rm eff}}{3}\int^{\Lambda} \frac{d^4k}{(2\pi)^4}\frac{M}{k^2+M^2}\,, \tag{5}$$

where M is the dynamical quark mass. Using $d^4k = (1/2)k^2dk^2\sin^2\theta d\theta \sin\phi d\phi d\psi$, performing the trivial regular integration's and using the variable $s = k^2$, the above expression reduces to:

$$M_f = m + \frac{\alpha_{\rm eff}M}{8\pi^2}\int_0^\infty ds\frac{s}{s+M^2} \tag{6}$$

The integral in Eq. (6) is divergent and we need to regularize it through proper-time regularization scheme [33] as:

$$\frac{1}{s+M^2} = \int_0^\infty d\tau {\rm e}^{-\tau(s+M^2)} \to \int_{\tau_{uv}^2}^{\tau_{ir}^2} d\tau {\rm e}^{-\tau(s+M^2)} = \frac{{\rm e}^{-\tau_{uv}^2(s+M^2)} - {\rm e}^{-\tau_{ir}^2(s+M^2)}}{s+M^2}. \tag{7}$$

Here, $\tau_{uv}^{-1} = \Lambda_{uv}$ is an ultra-violet regulator, which plays the dynamic role. The $\tau_{ir}^{-1} = \Lambda_{ir}$ stands for the infrared regulator whose non-zero value implements confinement by ensuring the absence of quarks production thresholds [37]. Hence, τ_{ir} is corresponds to the confinement scale [17]. Upon using this regularization procedure, the quadratic and logarithmic divergences remove and the axial-vector Ward-Takahashi identity [38, 39] is satisfied. The Eq. (7) represents that the location of the pole is at $s = -M^2$, which is cancelled by the numerator. In this way, the singularities have been removed and hence, the propagator is free from real as well as the complex poles, which is according to the definition of confinement *i.e.*, "an excitation described by a pole-less propagator would never reach its mass-shell" [40]. It should be noted that the confinement and chiral symmetry breaking occurs simultaneously in this model [41].

After performing integration we have:

$$M = m + \frac{M^3\alpha_{\rm eff}}{8\pi^2}\Gamma\left(-1, \tau_{uv}^2M^2, \tau_{ir}^2M^2\right)\,, \tag{8}$$

where

$$\Gamma(a,z_1,z_2) = \Gamma(a,z_1) - \Gamma(a,z_2)\,, \tag{9}$$

with

$$\Gamma(a,z) = \int_x^\infty t^{\alpha-1}{\rm e}^{-t}dt,$$

is the incomplete Gamma function. With a particular choice of parameters of Ref. [34], *i.e.*, $\tau_{ir} = (0.24\ {\rm GeV})^{-1}$ and $\tau_{uv} = (0.905\ {\rm GeV})^{-1}$, with the bare quark $m_u = m_d = 0.007$ GeV, from the numerical solution of the gap equation Eq. (8), we get the dynamical mass $M_u = M_d = 0.367$ GeV.

3. Gap equation in the presence of eE and eB at zero T

In QCD Lagrangian, the electromagnetic field A_μ^{ext} embedded in the covariant derivative as,

$$D_\mu = \partial_\mu - iQ_fA_\mu^{\rm ext}, \tag{10}$$

with $Q_f = (q_u = +2/3, q_d = -1/3)e$ is refers to the electric charges of u and d-quark respectively. Where With a particular choice of t the symmetric gauge vector potential $A_\mu^{ext} = (iEz, 0, -Bx, 0)$ in which electric and magnetic field are chosen along the z-axis. The gap equation in the presence of electric and magnetic field continues to be of the form Eq. (4) but now dressed with the electric and magnetic Schwinger propagator *i.e.*,$S_f(k) \to \tilde{S}_f(k)$ [1,2,4,20,24,33]. Thus, the final expression for the gap equation in the presence of background fields is given as [18]:

$$\tilde{M} = m + \frac{\alpha_{\rm eff}}{3\pi^2}\sum_{f=u,d}\int_{\tau_{uv}^2}^{\tilde{\tau}_{ir}^2} d\tau\tilde{M}{\rm e}^{-\tau\tilde{M}^2} \times\left[\frac{|Q_fE|}{\tan(|Q_fE|\tau)}\frac{|Q_fB|}{\tanh(|Q_fB|\tau)}\right]. \tag{11}$$

The confinement scale now slightly varies with the background fields:

$$\tilde{\tau}_{ir} = \tau_{ir}\frac{M_f}{\tilde{M}_f}, \tag{12}$$

where M is the dynamical mass without background fields and $\tilde{M}_f$ is the electric and magnetic field dependent dynamical mass. When both the fields eE, $eB \to 0$, the Eq. (11) reduces back to Eq. (8). The gap equation for a pure electric field can be obtained by setting $eB \to 0$, while for a pure magnetic field, $eE \to 0$. The numerical solution of the gap equation Eq. (11) as a function of eB for fixed values of eE has been discussed in detail in Ref. [18], which shows that in pure electric background the dynamical quark mass $\tilde{M}$ and the confining scale $\tilde{\tau}$ decreases as we increase the eE (*i.e.*, the chiral inhibition effect), whereas in the pure magnetic background the dynamical mass $\tilde{M}$ and the confining length scale $\tilde{\tau}$ increases (*i.e.*, Magnetic catalysis effect). Thus, we can say that the electric field tends to strengthen the restoration of the chiral symmetry whereas the magnetic field enhances the chiral symmetry breaking. When both fields are present, the strong competition occurred between them *i.e.*, the magnetic field enhances the dynamical mass while the electric suppresses it and vice versa. The pseudo- critical electric field $eE_c^{\chi,C}$ for the chiral symmetry breaking-restoration and confinement-deconfinement can be obtained from the electric gradient of the quark -antiquark condensate and the confining scale.

4. Phase diagram at $T \neq 0$ and in the presence of eE and eB

In this section, we discuss the expression for the gap equation and its numerical solution at finite temperature and in the presence of the background fields and explain how the dynamical mass and the confinement length scale behave at finite temperature and in the presence of electric and magnetic fields. The finite T version of the gap equation Eq. (5) in the presence of electric field eE and magnetic field eB is given by [18]

$$\hat{M} = m + \frac{\alpha_{\rm eff}}{3\pi^2}\sum_{f=u,d}\int_{\tau_{uv}^2}^{\hat{\tau}_{ir}^2} d\tau \hat{M} \mathrm{e}^{-\tau\hat{M}^2} \times \Theta_3\left(\frac{\pi}{2}, \mathrm{e}^{-\frac{|Q_f E|}{4T^2\tan(|Q_f E|\tau)}}\right) \times \left[\frac{|Q_f E|}{\tan(|Q_f E|\tau)}\frac{|Q_f B|}{\tanh(|Q_f B|\tau)}\right], \tag{13}$$

with $\Theta_3(\pi/2, e^{-x})$, is the third Jacobi's theta function . The confinement scale $\hat{\tau}_{ir}$ is now slightly vary with T, eE and eB is of the form:

$$\hat{\tau}_{ir} = \tau_{ir}\frac{M}{\hat{M}}. \tag{14}$$

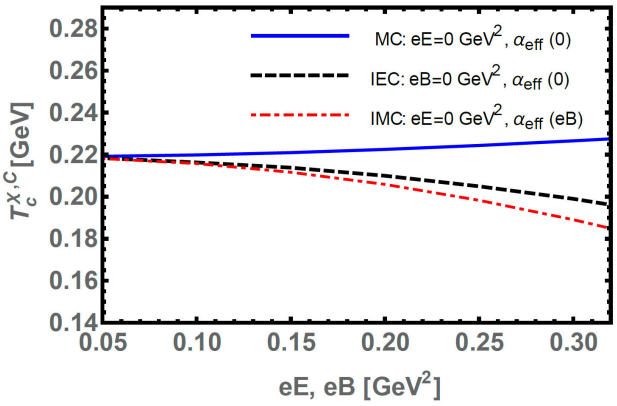

FIGURE 1. The phase diagram shows all the three phenomena MC, IMC and IE in the $T_c^{\chi,C} - (eE, eB)$ plane.

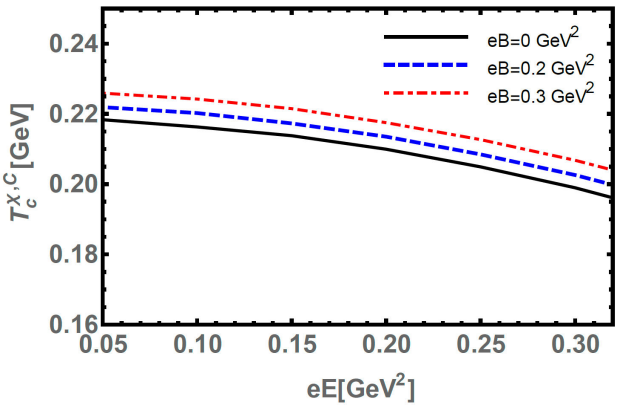

FIGURE 2. The phase diagram shows the inverse electric catalysis in the $T_c^{\chi,C}$–eE plane for various given values of eB. Here eE inhibits while eB facilitates the phase transition and hence yields the inverse electromagnetic catalysis.

Here $M = M(0,0,0)$ is the dynamical mass at $eB = eE = T = 0$, whereas $\hat{M} = M(eE, eB, T)$ is the variation of dynamical mass at finite eB, eE and T. To observe the pattern of inverse electric catalysis (IE), magnetic catalysis (MC), inverse magnetic catalysis (IMC) as shown in the Fig. 1 and electromagnetic inverse catalysis (IEMC) as shown in the Fig. 2 and 3, we compute the thermal gradient of the quark-antiquark condensate and the confining length scale for increasing values of eE, eB, and T. Thus, it can be seen that increasing temperature requires larger eB to catalyze the dynamical chiral symmetry breaking and confinement (MC), contrary to the case of eE, where increasing temperature requires smaller values of eE for anti-catalyze (IE) the dynamical chiral symmetry restoration and deconfinement. Upon taking into account the effect of the eB in the functional form of the effective coupling [17–19], where the effective coupling decreases with increasing eB, we thus produced the inverse magnetic catalysis (IMC) as shown in the Fig. 1.

Whereas, in the pure electric field eE background and at finite T, the solution of the gap equation supports the inverse electric catalysis effect. When both eE and eB are taken into

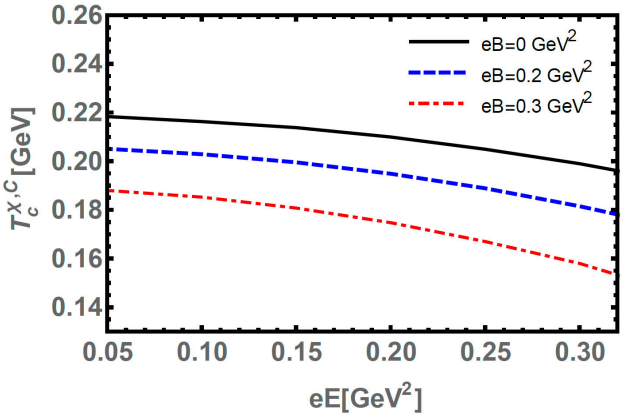

FIGURE 3. The phase diagram in the $T_c^{\chi,C} - eE$ Plane for various given values of eB with eB-dependent coupling [17, 18]. Here both fields eE and eB inhibits the phase transition and thus, we have found the IEMC.

account without Fig. 2 and with the magnetic field effective coupling Fig. 3, the critical $T_\chi^{c,C}$ for the chiral phase transition decreases, and hence we predict the electromagnetic inverse catalysis effect [18].

5. Conclusions

We have studied the QCD gap equation using symmetry preserving contact interaction model of quarks in the presence of the electric and magnetic field background and at finite temperature and conclude that: 1) In the zero temperature case, The magnetic field played the role of facilitator of the dynamical chiral symmetry breaking and confinement, Whereas the electric field acted as an inhibitor of the chiral symmetry breaking and confinement. 2) At finite temperature, the solution of our gap equation supports the phenomenon of magnetic catalysis and inverse magnetic catalysis when the effective coupling has taken to be decreasing function of the magnetic field. 3) At zero and finite temperature, and in pure electric case, we found the chiral inhibition effect or inverse electric catalysis effect. 4) At finite temperature, when both eE and eB are considered the critical temperature, we also observe the inverse electromagnetic catalysis effect with and without magnetic field-dependent effective coupling of the model.

Acknowledgments

I acknowledge the organizers of XVIII Mexican Workshop on Particles and Fields- 2022, for providing a conducive environment for the exchange of ideas during the presentation of this work, which led to the genesis of this manuscript.

1. S. P. Klevansky and R. H. Lemmer, Chiral symmetry breaking at finite temperatures, *Phys. Rev. D* **38** (1988) 3559, https://doi.org/10.1103/PhysRevD.38.3559.
2. H. Suganuma and T. Tatsumi, On the Behavior of Symmetry and Phase Transitions in a Strong Electromagnetic Field, *Annals Phys.* **208** (1991) 470, https://doi.org/10.1016/0003-4916(91)90304-Q.
3. K. G. Klimenko, Three-dimensional Gross-Neveu model in an external magnetic field, *Theor. Math. Phys.* **89** (1992) 1161, https://doi.org/10.1007/BF01015908.
4. S. P. Klevansky, The Nambu-Jona-Lasinio model of quantum chromodynamics, *Rev. Mod. Phys.* **64** (1992) 649, https://doi.org/10.1103/RevModPhys.64.649.
5. I. V. Krive and S. A. Naftulin, Dynamical symmetry breaking and phase transitions in a three-dimensional Gross-Neveu model in a strong magnetic field, *Phys. Rev. D* **46** (1992) 2737, https://doi.org/10.1103/PhysRevD.46.2737.
6. V. P. Gusynin, V. A. Miransky, and I. A. Shovkovy, Catalysis of dynamical flavor symmetry breaking by a magnetic field in (2+1)-dimensions, *Phys. Rev. Lett.* **73** (1994) 3499, https://doi.org/10.1103/PhysRevLett.76.1005., https://doi.org/10.1103/PhysRevLett.73.3499.
7. V. P. Gusynin, V. A. Miransky, and I. A. Shovkovy, Dynamical flavor symmetry breaking by a magnetic field in (2+1)- dimensions, *Phys. Rev. D* **52** (1995) 4718, https://doi.org/10.1103/PhysRevD.52.4718.
8. V. P. Gusynin, V. A. Miransky, and I. A. Shovkovy, Dimensional reduction and dynamical chiral symmetry breaking by a magnetic field in (3+1)-dimensions, *Phys. Lett. B* **349** (1995) 477, https://doi.org/10.1016/0370-2693(95)00232-A.
9. K. G. Klimenko, Three-dimensional Gross-Neveu model at nonzero temperature and in an external magnetic field, *Theor. Math. Phys.* **90** (1992) 1, https://doi.org/10.1007/BF01018812.
10. G. S. Bali *et al.*, The finite temperature QCD transition in external magnetic fields, *PoS LATTICE* **2011** (2011) 192, https://doi.org/10.22323/1.139.0192.
11. G. S. Bali *et al.*, Magnetic field-induced gluonic (inverse) catalysis and pressure (an)isotropy in QCD, *JHEP* **04** (2013) 130, https://doi.org/10.1007/JHEP04(2013)130.
12. G. Endrodi *et al.*, Magnetic catalysis and inverse catalysis for heavy pions, *JHEP* **07** (2019) 007, https://doi.org/10.1007/JHEP07(2019)007.
13. R. L. S. Farias *et al.*, Importance of asymptotic freedom for the pseudocritical temperature in magnetized quark matter, *Phys. Rev. C* **90** (2014) 025203, https://doi.org/10.1103/PhysRevC.90.025203.

14. P. Costa et al., Influence of the inverse magnetic catalysis and the vector interaction in the location of the critical end point, *Phys. Rev. D* **92** (2015) 036012, https://doi.org/10.1103/PhysRevD.92.036012.

15. E. J. Ferrer, V. de la Incera, and X. J. Wen, Quark Antiscreening at Strong Magnetic Field and Inverse Magnetic Catalysis, *Phys. Rev. D* **91** (2015) 054006, https://doi.org/10.1103/PhysRevD.91.054006.

16. A. Ayala *et al*., Inverse magnetic catalysis from the properties of the QCD coupling in a magnetic field, *Phys. Lett. B* **759** (2016) 99, https://doi.org/10.1016/j.physletb.2016.05.058.

17. A. Ahmad and A. Raya, Inverse magnetic catalysis and confinement within a contact interaction model for quarks, *J. Phys. G* **43** (2016) 065002, https://doi.org/10.1088/0954-3899/43/6/065002.

18. A. Ahmad, Chiral symmetry restoration and deconfinement in the contact interaction model of quarks with parallel electric and magnetic fields, *Chin. Phys. C* **45** (2021) 073109, https://doi.org/10.1088/1674-1137/abfb5f.

19. A. Ahmad *et al.*, Flavor, temperature and magnetic field dependence of the QCD phase diagram: magnetic catalysis and its inverse, *J. Phys. G* **48** (2021) 075002, https://doi.org/10.1088/1361-6471/abd88f.

20. G. Cao and X.-G. Huang, Chiral phase transition and Schwinger mechanism in a pure electric field, *Phys. Rev. D* **93** (2016) 016007, https://doi.org/10.1103/PhysRevD.93.016007.

21. W. R. Tavares and S. S. Avancini, Schwinger mechanism in the SU(3) Nambu-Jona-Lasinio model with an electric field, *Phys. Rev. D* **97** (2018) 094001, https://doi.org/10.1103/PhysRevD.97.094001.

22. M. Ruggieri and G. X. Peng, Quark matter in a parallel electric and magnetic field background: Chiral phase transition and equilibration of chiral density, *Phys. Rev. D* **93** (2016) 094021, https://doi.org/10.1103/PhysRevD.93.094021.

23. A. Ahmad and A. Farooq, Schwinger Pair Production in QCD from Flavor-Dependent Contact Interaction Model of Quarks (2023)

24. L. Wang and G. Cao, Competition between magnetic catalysis effect and chiral rotation effect, *Phys. Rev. D* **97** (2018) 034014, https://doi.org/10.1103/PhysRevD.97.034014.

25. W. R. Tavares, R. L. S. Farias, and S. S. Avancini, Deconfinement and chiral phase transitions in quark matter with a strong electric field, *Phys. Rev. D* **101** (2020) 016017, https://doi.org/10.1103/PhysRevD.101.016017.

26. A. Bzdak and V. Skokov, Event-by-event fluctuations of magnetic and electric fields in heavy ion collisions, *Phys. Lett. B* **710** (2012) 171, https://doi.org/10.1016/j.physletb.2012.02.065.

27. W.-T. Deng and X.-G. Huang, Event-by-event generation of electromagnetic fields in heavy-ion collisions, *Phys. Rev. C* **85** (2012) 044907, https://doi.org/10.1103/PhysRevC.85.044907.

28. J. Bloczynski *et al*., Azimuthally fluctuating magnetic field and its impacts on observables in heavy-ion collisions, *Phys. Lett. B* **718** (2013) 1529, https://doi.org/10.1016/j.physletb.2012.12.030.

29. J. Bloczynski *et al*., Charge-dependent azimuthal correlations from AuAu to UU collisions, *Nucl. Phys. A* **939** (2015) 85, https://doi.org/10.1016/j.nuclphysa.2015.03.012.

30. L. Wang *et al*., Nambu-Jona-Lasinio model in a parallel electromagnetic field, *Phys. Lett. B* **780** (2018) 273, https://doi.org/10.1016/j.physletb.2018.03.018.

31. G. Cao, Effects of a parallel electromagnetic field in the threeflavor Nambu-Jona-Lasinio model, *Phys. Rev. D* **101** (2020) 094027, https://doi.org/10.1103/PhysRevD.101.094027.

32. H. L. L. Roberts *et al.*, pi- and rho-mesons, and their diquark partners, from a contact interaction, *Phys. Rev. C* **83** (2011) 065206, https://doi.org/10.1103/PhysRevC.83.065206.

33. J. S. Schwinger, On gauge invariance and vacuum polarization, *Phys. Rev.* **82** (1951) 664, https://doi.org/10.1103/PhysRev.82.664.

34. L. X. Gutierrez-Guerrero *et al*., Pion form factor from a contact interaction, *Phys. Rev. C* **81** (2010) 065202, https://doi.org/10.1103/PhysRevC.81.065202.

35. P. Boucaud *et al*., The Infrared Behaviour of the Pure Yang-Mills Green Functions, *Few Body Syst.* **53** (2012) 387, https://doi.org/10.1007/s00601-011-0301-2.

36. A. Ahmad and A. Murad, Color-flavor dependence of the Nambu-Jona-Lasinio model and QCD phase diagram, *Chin. Phys. C* **46** (2022) 083109, https://doi.org/10.1088/1674-1137/ac6cd8.

37. C. D. Roberts *et al*., Aspects of hadron physics, *Eur. Phys. J. ST* **140** (2007) 53, https://doi.org/10.1140/epjst/e2007-00003-5.

38. J. C. Ward, An Identity in Quantum Electrodynamics, *Phys. Rev.* **78** (1950) 182, https://doi.org/10.1103/PhysRev.78.182.

39. Y. Takahashi, On the generalized Ward identity, *Nuovo Cim.* **6** (1957) 371, https://doi.org/10.1007/BF02832514.

40. D. Ebert, T. Feldmann, and H. Reinhardt, Extended NJL model for light and heavy mesons without q - anti-q thresholds, *Phys. Lett. B* **388** (1996) 154, https://doi.org/10.1016/0370-2693(96)01158-6.

41. F. Marquez et al., The dual quark condensate in local and nonlocal NJL models: an order parameter for deconfinement?, *Phys. Lett. B* **747** (2015) 529, https://doi.org/10.1016/j.physletb.2015.06.031.